Jacquey, A. B., Cacace, M., Blöcher, G. (2017): Modelling coupled fluid flow and heat transfer in fractured reservoirs: description of a 3D benchmark numerical case. - *Energy Procedia*, *125*, pp. 612—621.

DOI: http://doi.org/10.1016/j.egypro.2017.08.227

Available online at www.sciencedirect.com

ScienceDirect

Energy Procedia 125 (2017) 612–621

Energy Procedia

www.elsevier.com/locate/procedia

European Geosciences Union General Assembly 2017, EGU Division Energy, Resources & Environment, ERE

Modelling coupled fluid flow and heat transfer in fractured reservoirs: description of a 3D benchmark numerical case

Antoine B. Jacquey[a,b,*], Mauro Cacace[a], Guido Blöcher[a]

[a]*GFZ German Research Centre for Geosciences, Telegrafenberg, 14473 Potsdam, Germany*
[b]*RWTH Aachen University, Templergraben 55, 52056 Aachen, Germany*

Abstract

One challenge of modelling coupled fluid flow and heat transfer within geological reservoirs lies in representing the geometry of fractures and to formulate the physics of their hydraulic behaviours. This contribution presents a 3D case to be used to test the ability of simulators in solving for such issues. The reliability of the study is tested against three simulators (GOLEM, OpenGeosys, and Feflow), which integrates fractures as single-nodded lower dimensional elements embedded in the rock matrix. Comparing the results we can conclude on the validity of the synthetic model as a code benchmarking case for simulators adopting a similar approach.

Peer-review under responsibility of the scientific committee of the European Geosciences Union (EGU) General Assembly 2017 – Division Energy, Resources and the Environment (ERE).

Keywords: Coupled fluid flow and heat transfer; Fractured reservoirs; Numerical simulation; Finite Element Method

1. Introduction

Understanding the coupling among physical processes occurring within fractured reservoirs is an important subject for several geotechnical applications involving utilisation of the resources (e.g. geothermal energy extraction or enhanced oil recovery) [1, 2, 3] or subsurface storage facilities (e.g. CO_2 storage or nuclear waste repository) [4, 5]. In particular, the hydraulic and thermal states of a reservoir are essential system state variables that must be correctly quantified either because these are the first order controlling processes of a natural system (for example for geothermal reservoir applications) or because they do exert a control on other primary processes via thermodynamic state system equations (for example, pressure and temperature conditions controlling the kinematics of reactive and reactant flow and transport processes or mechanical processes) [6, 7, 3]. In such a context, numerical modelling has become a stan-

* Corresponding author. Tel.: +49–331–288–1779; fax: +49–331–288–2825
E-mail address: antoine.jacquey@gfz-potsdam.de

1876-6102
Peer-review under responsibility of the scientific committee of the European Geosciences Union (EGU) General Assembly 2017 – Division Energy, Resources and the Environment (ERE).
10.1016/j.egypro.2017.08.227

dard practice to predict and quantify the evolution in time of the pore pressure and temperature distributions during geotechnical operations [8, 9].

Nomenclature

p_f	Pore pressure [Pa].
T	Temperature [K].
n	Porosity [-].
$\rho_{f,s,b}$	Fluid/Solid/Bulk density [kg m^{-3}].
$c_{f,s,b}$	Fluid/Solid/Bulk heat capacity [J kg^{-1} K^{-1}].
K_f	Fluid modulus [Pa].
$\lambda_{f,s,b}$	Fluid/Solid/Bulk thermal conductivity [W m^{-1} K^{-1}].
$\boldsymbol{v}_f$	Fluid velocity [m s^{-1}].
$\boldsymbol{q}_D$	Darcy's velocity [m s^{-1}].
$\boldsymbol{q}_T$	Thermal flux [W m^{-2}].
$\boldsymbol{k}$	Permeability tensor [m^2].
μ_f	Fluid dynamic viscosity [Pa s].
$\boldsymbol{g}$	Gravity vector [m s^{-2}].
b	Effective fracture aperture [m].

The presence of geological heterogeneities such as fractures and faults within a reservoir increases the complexity of the modelling strategy by giving rise to a multiscale and nonlinear system. In order to tackle these issues, different approaches are usually adopted in the modelling community [10]. A first class of modelling approaches relies on a three-dimensional representation of faults and fractures as an equivalent porous medium (EPM) with heterogeneous properties. The main advantage of such an approach stems from numerically integrating complex multi-coupled behaviours without adding additional costs on the model geometry and on the physical processes simulated. However, this approach can also lead to a considerable increase of the degrees of freedom due to the full geometrical discretisation of the fracture volume. Furthermore, high gradients of elements sizes at the interface between the EPM (typically of an order ranging from μm to cm) and the porous matrix (order of m for a typical reservoir application) can occur and have impacts on the efficiency, stability, and accuracy of the numerical solutions.

As an alternative, several numerical simulators chose to represent explicitly the fractures and faults as discontinuities in the rock matrix by making use of lower dimensional elements of zero effective thickness (single or higher order nodded elements depending on the particular application) embedded in the porous matrix (for example, 2D elements in a 3D matrix to represent fractures) [11, 12, 13]. The main advantage of this method is to represent the discontinuity resulting from the presence of these structures without increasing considerably the number of degrees of freedom of the problem. However, it requires some additional efforts in the discretisation process to maintain internal geometric consistency between the fracture and matrix elements. In addition, such a geometrical representation requires a specific numerical implementation of the physical behaviour of these discrete heterogeneities and their direct coupling with the one of the porous matrix [14, 15].

Recently, different approaches have been presented that enable to a varying degree the integration of such discontinuous elements into a consistent Finite Element representation of the fractured porous medium. An example of such approaches is given by the open software MeshIt [13], which will be used in the present study. Based and linked to the aforementioned meshing software, a novel simulator called GOLEM has been developed based on the MOOSE Framework for modelling coupled thermal-hydraulic-mechanical processes in fractured rocks in a flexible manner using a full implicit coupling [15].

In this contribution, we propose a synthetic and relative simple study case which can be used in order to test the ability and reliability of existing numerical simulators to address coupled fluid flow and transport processes in porous media in the presence of discrete heterogeneities as fractures and fault zones. Therefore, in a first part we present in some details the mathematical formulation of the problem, where we focus only in the transport of heat, though the same approach can be used to described the transport of any non-reactant solutal component. In addition, some

details of the numerical implementation of the resulting coupled systems of equations are also provided. Extensive information of the numerics can be found in the related literature, e.g. [14, 15].

In a second part, the synthetic model is presented. The aim here is to propose a relatively simplistic, though physically sound study which can be used as a benchmark case for any other modelling platform adopting a similar approach to represent fractured porous media. Therefore, the results obtained by making use of three different numerical simulators (two open source, i.e. GOLEM and OpenGeoSys and one commercial FEFLOW©) are compared, thus verifying the reliability of the proposed benchmark study.

2. Problem formulation and numerical implementation

In the following, the governing equations for fluid flow and heat transfer within porous rocks and discrete fractures are briefly described. Their derivation is based on the fluid mass balance, the energy balance of the solid-fluid mixture and on the conservation of fluid momentum. More details can be found in [15]. In this contribution, non-deformable porous media fully filled with water are considered thought the GOLEM simulator can also consider (in)-elastic mechanical feedbacks. In a similar fashion, we do not explicitly consider variation in the fluid properties as a function of the system primary unknowns. For a complete description of the system of equations the reader is referred to [15]. Fractures and faults are represented as discrete features and their geometry is considered via lower dimensional elements embedded in the porous matrix filled with water.

2.1. Governing equations for the porous matrix

Within a non-deformable porous matrix, the pore pressure distribution is governed by the following equation:

$$\frac{n}{K_f}\frac{\partial p_f}{\partial t} + \nabla \cdot \boldsymbol{q}_D = 0. \tag{1}$$

The Darcy's law is used to describe the conservation of fluid momentum and relates the fluid velocity to the pore pressure variable:

$$\boldsymbol{q}_D = n\boldsymbol{v}_f = -\frac{\boldsymbol{k}}{\mu_f} \cdot \left(\nabla p_f - \rho_f \boldsymbol{g}\right). \tag{2}$$

The temperature distribution is based on the energy balance of the solid-fluid mixture assuming local thermal equilibrium between the two phases ($T_s = T_f = T$):

$$(\rho c)_b \frac{\partial T}{\partial t} + \nabla \cdot \boldsymbol{q}_T = 0 \tag{3}$$

where $\boldsymbol{q}_T$ describes the heat flux considering both diffusive and advective processes:

$$\boldsymbol{q}_T = \rho_f c_f \boldsymbol{q}_D T - \lambda_b \nabla T. \tag{4}$$

2.2. Governing equations for the discrete fractures

In the current approach, fractures are explicitly represented by using single-noded, zero thickness finite elements. These elements are assumed to be clean (e.g. no asperities are considered in their geometric description) and fully saturated ($n = 1$) and can be parameterised based on their effective aperture, which is used as weighing parameter and provides a quantitative measure of the geometric width of the fracture plane.

In the following, the governing equations for fluid flow and heat transfer within fractures are briefly described as based on [14, 15]. It is worth mentioning that we do not distinguish in the current approach between mechanical and hydraulic apertures of the fracture plane (both considered constant in the present study) because of lack of data to constrain the differences between these two effective apertures.

The pore pressure within the fracture plane is governed by the following equation:

$$\frac{b}{K_f}\frac{\partial p_f}{\partial t} + \bar{\nabla} \cdot (b\bar{\boldsymbol{q}}_D) = 0 \tag{5}$$

where the $\bar{\nabla}\cdot$ symbol denotes the divergence operator in the local coordinate system of the fracture plane. The fluid flow within the fracture plane is also written in the local coordinate system as follows:

$$\bar{\boldsymbol{q}}_D = -\frac{\bar{\boldsymbol{k}}}{\mu_f} \cdot \left(\bar{\nabla} p_f - \rho_f \boldsymbol{g}\right) \tag{6}$$

where $\bar{\nabla} p_f$ is the gradient of pore pressure and $\bar{\boldsymbol{k}}$ the permeability tensor in the local coordinate system. Laminar flow within the fracture plane can be assumed by using the cubic law (or parallel plate concept) [16, 17, 18]. In that case the permeability tensor in local coordinates is expressed as:

$$\bar{\boldsymbol{k}} = \frac{b^2}{12}\bar{\boldsymbol{I}} \tag{7}$$

where $\bar{\boldsymbol{I}}$ is the unit tensor in local coordinates. The temperature distribution is governed by the energy balance in the discrete fracture as follow:

$$b\rho_f c_f \frac{\partial T}{\partial t} + \bar{\nabla} \cdot \bar{\boldsymbol{q}}_T = 0 \tag{8}$$

where the heat flux in local coordinates $\bar{\boldsymbol{q}}_T$ is defined as:

$$\bar{\boldsymbol{q}}_T = b\rho_f c_f \bar{\boldsymbol{q}}_D T - b\lambda_f \bar{\nabla} T \tag{9}$$

including as well both diffusive and advective processes.

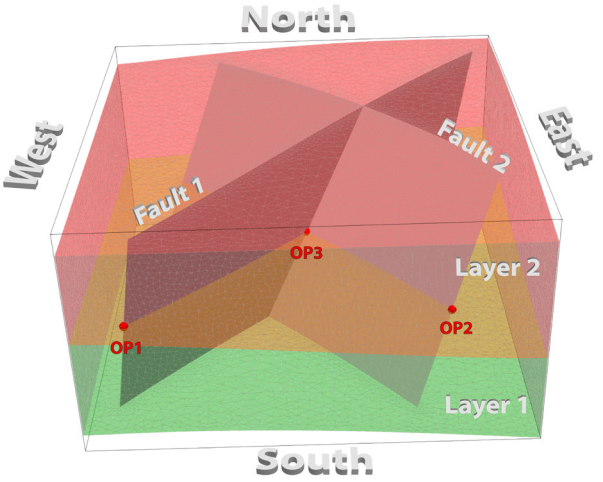

Fig. 1. Geometry of the problem. The domain contains two intersecting faults embedded in a two-layered porous matrix. Three observation points (OP) which locations are marked in the figure (on the faults planes) are used to illustrate the results.

2.3. Rotational matrix

In the current numerical implementation, we make use of standard coordinate transformation with the Jacobian matrix of the mapping between global (x_i) and local (x'_i) coordinate systems to compute the derivatives of the test functions and the direction-dependent material properties (permeability tensor for example). The transformation in local coordinates for the lower-dimensional elements is performed by computing the rotational matrix $\boldsymbol{R}$ as follows:

$$\boldsymbol{R} = \begin{bmatrix} \cos(x', x) & \cos(x', y) & \cos(x', y) \\ \cos(y', x) & \cos(y', y) & \cos(y', y) \\ \cos(z', x) & \cos(z', y) & \cos(z', y) \end{bmatrix} \tag{10}$$

where $\cos\left(x'_i, x_i\right)$ are the directional cosines. This coordinate system transformation is applied to all direction-dependent material property as well as directional derivatives. For the permeability tensor for example, it gives:

$$\boldsymbol{k} = \boldsymbol{R}\bar{\boldsymbol{k}}\boldsymbol{R}^T. \tag{11}$$

3. Code benchmarking: two intersecting faults embedded in a two-layered matrix

The benchmark study case proposed in this study describes a synthetic model consisting of a two-layered porous medium in the presence of two intersecting planar faults. The geometry of the model is summarised in Figure 1. This setup is inspired by previous work from two of the authors [19, 20]. The horizontal extension of the domain is 200 m

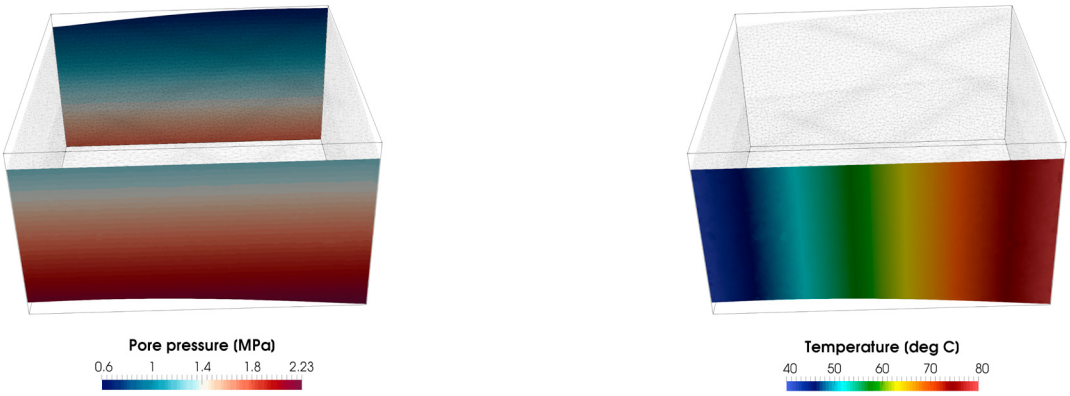

Fig. 2. Boundary conditions of the numerical problem. (Left) Fixed pore pressure boundary conditions on the southern and northern boundaries; (Right) Fixed temperature on the southern boundary viewed from the southern boundary.

and the vertical one is 100 m. All data, comprising the meshes adopted, and input files are available upon request by contacting the corresponding author.

In order to test the reliability of the proposed study case as a benchmark study, three different simulators are considered in this study: the open-source GOLEM simulator [15], the open-source simulator OpenGeoSys v 5 [21] and the commercial simulator FEFLOW© v 7.0 [22], which can all solve coupled partial differential equations on unstructured meshes.

3.1. Setup of the problem

The model consists of simulating infiltration of water from the southern border into the model domain and by letting the inflowing water advecting as a non-isothermal front (here used as a passive flow trace) fixed along the same boundary. As initial conditions, a hydrostatic pore pressure distribution is assumed with a pore pressure of 1.5 MPa at the centre of the model (z = 0 m) as well as a homogeneous temperature distribution of 60 °C. A regional fluid flow with a pressure gradient of Δp_f = 0.5 MPa from the southern to the northern boundary is imposed via pore pressure boundary conditions. Across the southern boundary, a linear distribution of temperature increasing from west (40 °C) to east (80 °C) is applied. These boundary conditions are summarised in Figure 2. All results presented in the following paragraphs are based on an incompressible fluid saturating the pores. Additional simulations considered fluid density and fluid viscosity variations have been also carried out. However, given the setting, such variations in the fluid properties did not affect the final results. Therefore, for the sake of readiness, we decide not to discuss these additional results in the present manuscript. A more systematic study of buoyant flow of viscous fluid within a fractured porous medium is described in a companion paper in this special issue (Magri et al., this issue).

The aim of the modelling is to test the ability of the simulators to model water infiltration within the model domain and quantify the impacts of the two faults on the pore pressure and fluid velocity distributions. The simulations are considered under transient conditions, for approximately a total of 150 years allowing to visualise the dynamics of the coupled fluid flow and heat transfer as also influenced by the faults. The Finite Element mesh used for the simulations comprises 583 633 tetrahedral elements and 4387 triangular elements and was generated with the MeshIt software [13] for the three different simulators.

3.2. Overview of the results: 3D temperature and pressure distribution

Figure 3 illustrates the pore pressure field on a horizontal cross section and the distribution of several temperature isosurfaces at the end of the simulation conducted with the GOLEM simulator. The presence of the two faults influences the pore pressure distribution with the highest gradients of pore pressure located at the tips of the faults.

Table 1. Physical properties for the two faults embedded in a two-layered matrix model.

Property	SI unit	Layer 1	Layer 2	Fault 1	Fault 2
Average thickness/Aperture	m	55	45	0.05	0.05
Porosity	–	0.15	0.08	1	1
Fluid density	$\mathrm{kg\,m^{-3}}$	1000	1000	1000	1000
Solid density	$\mathrm{kg\,m^{-3}}$	2600	2600	–	–
Storage coefficient $\left(\frac{n}{K_f}\right)$	$\mathrm{Pa^{-1}}$	7.0×10^{-10}	7.0×10^{-10}	4.6×10^{-10}	4.6×10^{-10}
Permeability	$\mathrm{m^2}$	2.0×10^{-14}	1.0×10^{-14}	1.0×10^{-8}	5.0×10^{-9}
Fluid viscosity	Pa s	5.0×10^{-4}	5.0×10^{-4}	5.0×10^{-4}	5.0×10^{-4}
Fluid thermal conductivity	$\mathrm{W\,m^{-1}\,K^{-1}}$	0.65	0.65	0.65	0.65
Solid thermal conductivity	$\mathrm{W\,m^{-1}\,K^{-1}}$	3.0	3.0	–	–
Fluid heat capacity	$\mathrm{J\,kg^{-1}\,K^{-1}}$	4180	4180	4180	4180
Solid heat capacity	$\mathrm{J\,kg^{-1}\,K^{-1}}$	1000	1000	–	–

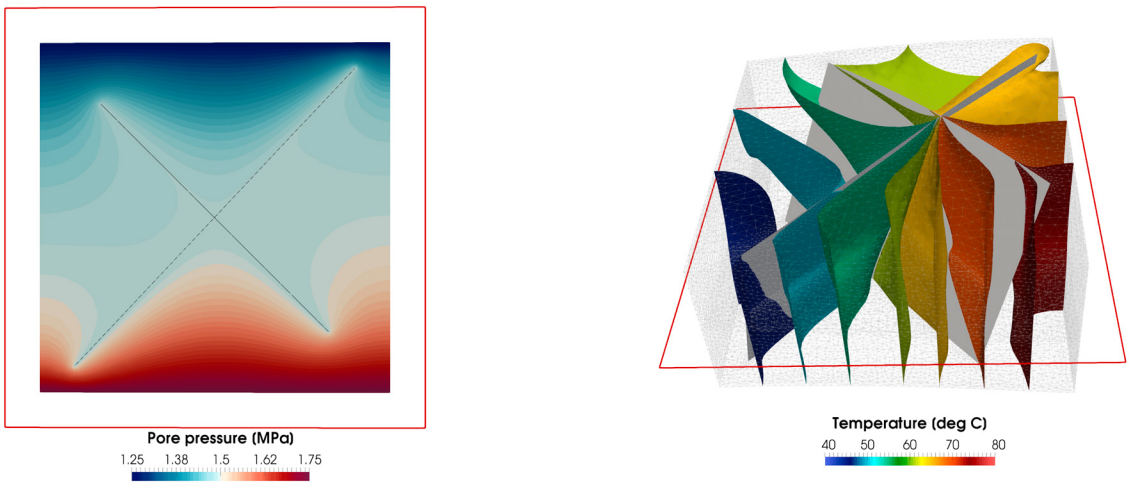

Fig. 3. Overview of the results at the end of the simulation (t = 150 years). (Left) Pore pressure distribution on a cross-section area at z = 0 m; (Right) Distribution of temperature isosurfaces viewed from the southern boundary. These figures illustrates the results obtained based on the GOLEM simulator.

Figure 3 depicts also the three-dimensional thermal field at the end of the simulation. Because of focused flow within the faults planes, higher pore pressure gradients are found along the planes of the faults leading to a mixing of cold and warm fluid at the intersection line of the two faults located approximately in the middle of the domain.

In the following, the results obtained from the three different simulators are compared in some details. The same unstructured mesh is used for all the simulations and the same simulation setup is considered for each simulator.

3.3. Simulators comparison

Figure 4 illustrates the evolution of pore pressure and temperature at the three observation points (OP) obtained by the three different simulators (see Figure 1). A similar pore pressure response is obtained by the three different simulators and no clear discrepancies can be noticed. The initial pore pressure is defined by the hydrostatic distribution prescribed as initial conditions. After several hours, the pore pressure at the three observation points decreases continuously due to pore pressure diffusion within the fault planes. It stabilises after about 10 simulated days to a

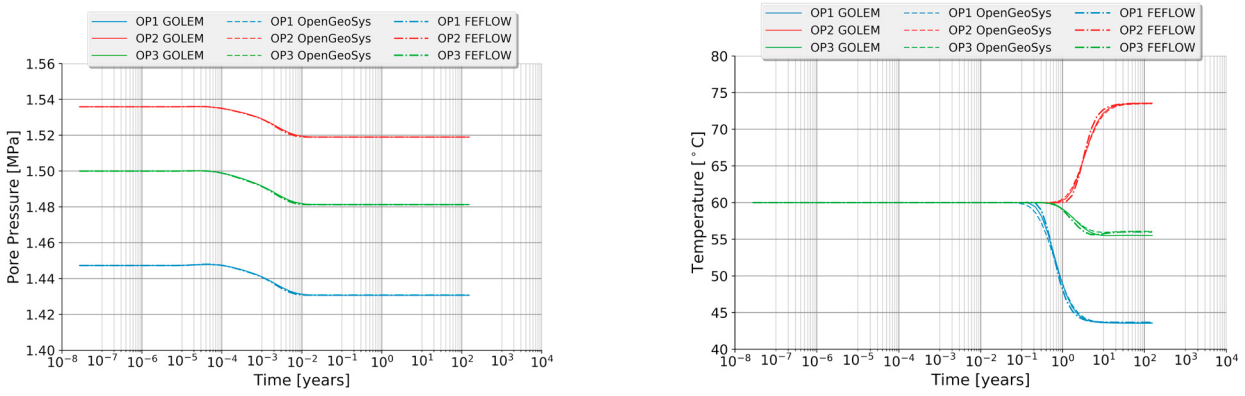

Fig. 4. Evolution of (left) pore pressure and (right) temperature at the three observation points whose locations are illustrated in Figure 1.

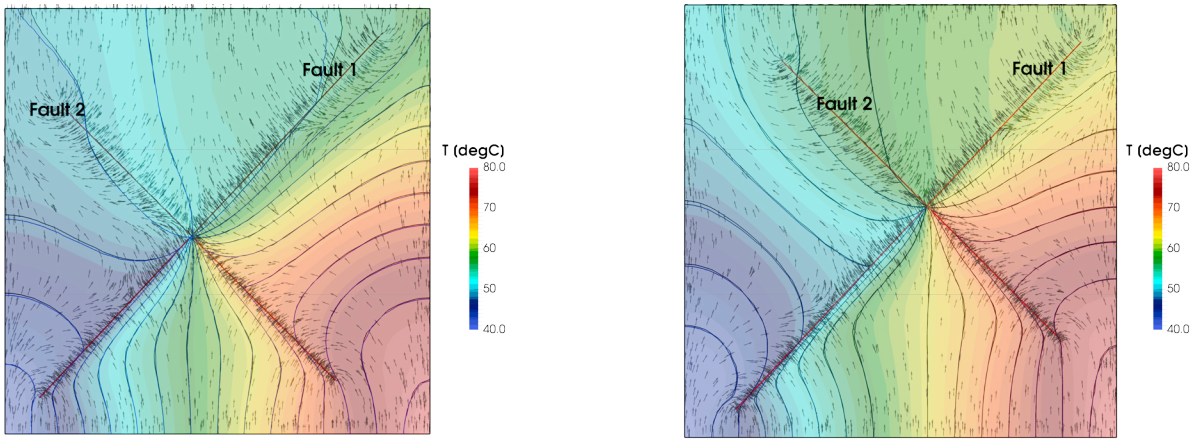

Fig. 5. Horizontal cross-sections at (left) $z = -25$ m and (right) $z = 25$ m illustrating the temperature distribution at the end of the simulation. Black lines show the isolines of temperature every 5 °C obtained with the GOLEM simulator and blue lines the ones obtained with the OpenGeoSys simulator. The temperature distribution plotted in the background is the one obtained with the GOLEM simulator.

final value 2 bars lower in magnitudes than its initial value. The temperature remains first constant at the initial value (60 °C) at the three observations points. After one simulated month, the temperature at OP1 starts to decrease due to the cold water front imposed as boundary condition which is advected by the most conductive fault (fault 1). After 10 simulated months, the temperature of the two other observation points (OP2 and OP3) starts also to deviate from the initial value. At the end of the simulation, the temperature at OP1 dropped to 44 °C, the one at OP2 increased to 73 °C and the one at OP3 decreased to 56 °C (the cold water front reaches OP3 before the warm water front because fault 1 is more conductive than fault 2). Though the time of the thermal front arrival at the three observation points is different (up to a minute in at OP1, see Figure 4), the overall thermal evolution remains similar.

Figure 5 illustrates the comparison of temperature distributions on horizontal cross-sections within the three-dimensional domain at $z = -25$ (left panel) and $z = 25$ m (right panel) for the simulators GOLEM and OpenGeoSys. The isolines of temperature (every 5 °C) obtained with the GOLEM simulator are illustrated in black and the ones obtained with the OpenGeoSys simulator in blue. The black and blue lines cannot be distinguished from one another and only minor differences between the two simulators can be noticed closed to the boundary of the domain (upper left).

Figure 6 shows the same illustrations as Figure 5 but with the blue lines corresponding to the isolines of temperature obtained with the FEFLOW© simulator. For both cross sections, differences between the FEFLOW© and GOLEM simulators can be noticed. For the lower cross-section (left panel of Figure 6), the highest differences are located prin-

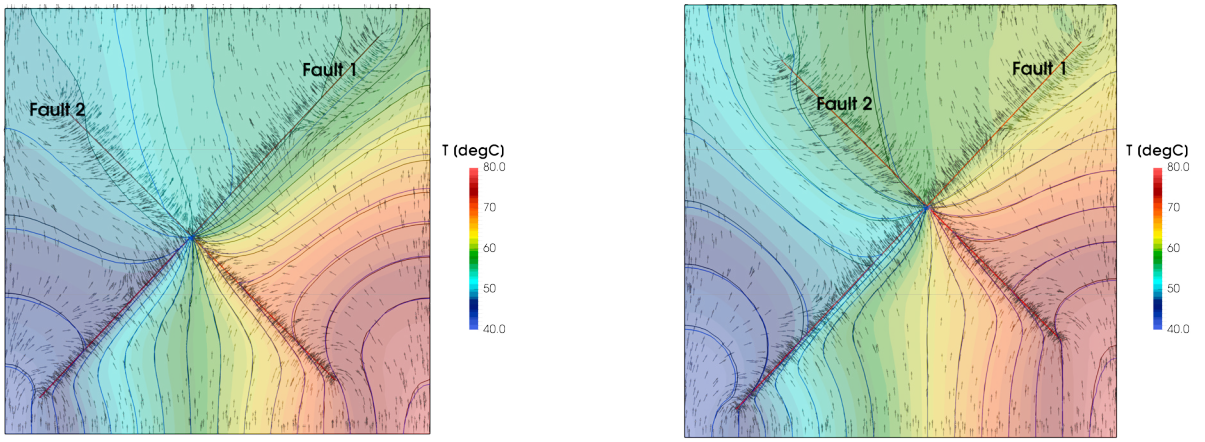

Fig. 6. Horizontal cross-sections at (left) $z = -25$ m and (right) $z = 25$ m illustrating the temperature distribution at the end of the simulation. Black lines show the isolines of temperature every 5 °C obtained with the GOLEM simulator and blue lines the ones obtained with the FEFLOW© simulator. The temperature distribution plotted in the background is the one obtained with the GOLEM simulator.

cipally within the left half of the domain (close to fault 1) where the front calculated with the FEFLOW© simulator is behind the one calculated with the GOLEM simulator. On the right half of the domain (close to fault 2), differences between the results of the two simulators decrease, though the thermal front calculated with the FEFLOW© simulator is running ahead of the one calculated with the GOLEM simulator. For the upper cross-section (right panel of Figure 6), the overall differences are smaller compared to the one of the lower cross-section with the same trend. In general, it can be noticed that the highest differences between the two simulators correspond to locations characterized by the highest ratio in modelled permeability, i,e. at the intersection points between the faults and the matrix. Furthermore, some instabilities in the temperature distribution can be noticed in the results obtained with the FEFLOW© simulator at the intersection of the two faults (as identified by the irregular shape of the blue contours).

4. Discussion and conclusions

In this contribution, we presented the theory and numerical implementation for modelling coupled fluid flow and heat transfer using zero-thickness lower dimensional elements for representing faults and fractures. We proposed a benchmark test case that can be used to validate the ability of numerical simulators to address issues related to groundwater and transport processes in porous media in the presence of existing fractures and faults. The relative geometrical complexity of the proposed benchmark test case allows to test the reliability of numerical simulators for geometrical and physical features which may be present in a field case application, such as intersecting faults, highly permeable faults or fractures compared to the rock matrix or the impact of gravity on the fluid flow in faults.

To validate the reliability of the discussed benchmark, three different numerical simulators have been considered and applied to the same problem and the results have been compared. Code benchmarking has been performed on a generic model comprising two intersecting faults in a two-layer domain by comparing the results obtained with the GOLEM simulator with the ones obtained with the open-source simulator OpenGeoSys and the commercial simulator FEFLOW©. The results obtained with the GOLEM and OpenGeoSys simulators are almost similar and only negligible differences were noticeable. Some discrepancies were found when comparing with the results obtained with the FEFLOW© simulator, especially in regions where the highest gradient of permeability between the three-dimensional matrix and the fracture is found. However, the reasons of these discrepancies with the FEFLOW© simulator results remain speculative at this stage as they are likely related to the specific details of the numerical implementation adopted to represent the faults and fractures within the framework of the FEFLOW© simulator.

The hydraulic behaviour of fractures and faults depends on the stress state acting on these structures. Furthermore, the presence of these heterogeneities may alter the regional stress field locally due to inelastic strain accumulation which may result in a different stress regime in the vicinity of a fault. It is therefore important to account for the

mechanical feedbacks induced by these geological heterogeneities such as frictional behaviour, opening or closing of fractures and faults to model realistic hydraulic behaviour. The current limitations of the single-noded lower dimensional elements representation is the impossibility to account for a jump in the primary variables nor their gradients (displacements or stresses for mechanical modelling) and therefore fracture and faults mechanics. These mechanical behaviours can be taken into account by improving the current approach, for example with local node enrichment for the mechanics and are the topic of ongoing activities.

References

[1] J. F. W. Gale, R. M. Reed, J. Holder, Natural fractures in the Barnett Shale and their importance for hydraulic fracture treatments, AAPG Bulletin 91 (4) (2007) 603–622.

[2] G. Blöcher, T. Reinsch, J. Henninges, H. Milsch, S. Regenspurg, J. Kummerow, H. Francke, S. Kranz, A. Saadat, G. Zimmermann, E. Huenges, Hydraulic history and current state of the deep geothermal reservoir Groß Schönebeck, Geothermics 63 (2016) 27–43.

[3] A. B. Jacquey, M. Cacace, G. Blöcher, N. Watanabe, E. Huenges, M. Scheck-Wenderoth, Thermo-poroelastic numerical modelling for enhanced geothermal system performance: Case study of the Groß Schönebeck reservoir, Tectonophysics 684 (2016) 119–130.

[4] P. Delage, Y. Cui, A. Tang, Clays in radioactive waste disposal, Journal of Rock Mechanics and Geotechnical Engineering 2 (2) (2010) 111–123.

[5] P. Bergmann, M. Diersch, J. Götz, M. Ivandic, A. Ivanova, C. Juhlin, J. Kummerow, A. Liebscher, S. Lüth, S. Meekes, B. Norden, C. Schmidt-Hattenberger, F. M. Wagner, F. Zhang, Review on geophysical monitoring of CO2 injection at Ketzin, Germany, Journal of Petroleum Science and Engineering 139 (2016) 112–136.

[6] M. De Lucia, T. Kempka, M. Kühn, A coupling alternative to reactive transport simulations for long-term prediction of chemical reactions in heterogeneous CO2 storage systems, Geoscientific Model Development 8 (2) (2015) 279–294.

[7] P. Klitzke, M. Luzi-Helbing, J. M. Schicks, M. Cacace, A. B. Jacquey, J. Sippel, M. Scheck-Wenderoth, J. I. Faleide, Gas Hydrate Stability Zone of the Barents Sea and Kara Sea Region, Energy Procedia 97 (2016) 302–309.

[8] M. Cacace, G. Blöcher, N. Watanabe, I. Moeck, N. Börsing, M. Scheck-Wenderoth, O. Kolditz, E. Huenges, Modelling of fractured carbonate reservoirs: outline of a novel technique via a case study from the Molasse Basin, southern Bavaria, Germany, Environmental Earth Sciences 70 (8) (2013) 3585–3602.

[9] H. Class, L. Mahl, W. Ahmed, B. Norden, M. Kühn, T. Kempka, Matching Pressure Measurements and Observed CO2 Arrival Times with Static and Dynamic Modelling at the Ketzin Storage site, Energy Procedia 76 (2015) 623–632.

[10] P. Dietrich, R. Helmig, M. Sauter, H. Hötzl, J. Köngeter, G. Teutsch (Eds.), Flow and Transport in Fractured Porous Media, Springer-Verlag, Berlin/Heidelberg, 2005.

[11] J. M. Segura, I. Carol, On zero-thickness interface elements for diffusion problems, International Journal for Numerical and Analytical Methods in Geomechanics 28 (9) (2004) 947–962.

[12] J. M. Segura, I. Carol, Coupled HM analysis using zero-thickness interface elements with double nodes. Part I: Theoretical model, International Journal for Numerical and Analytical Methods in Geomechanics 32 (18) (2008) 2083–2101.

[13] M. Cacace, G. Blöcher, MeshIt - a software for three dimensional volumetric meshing of complex faulted reservoirs, Environmental Earth Sciences 74 (6) (2015) 5191–5209.

[14] N. Watanabe, W. Wang, J. Taron, U. J. Görke, O. Kolditz, Lower-dimensional interface elements with local enrichment: application to coupled hydro-mechanical problems in discretely fractured porous media, International Journal for Numerical Methods in Engineering (2012) 1010–1034.

[15] M. Cacace, A. B. Jacquey, Flexible parallel implicit modelling of coupled Thermal-Hydraulic-Mechanical processes in fractured rocks, Solid Earth Discussions (2017) 1–33.

[16] D. T. Snow, Anisotropic Permeability of Fractured Media, Water Resources Research 5 (6) (1969) 1273–1289.

[17] R. Zimmerman, G. Bodvarsson, Hydraulic conductivity of rock fractures, Transport in Porous Media 23 (1) (1996) 1–30.

[18] D. J. Brush, N. R. Thomson, Fluid flow in synthetic rough-walled fractures: Navier-Stokes, Stokes, and local cubic law simulations, Water Resources Research 39 (4) (2003) 1084–1100.

[19] M. G. Blöcher, M. Cacace, B. Lewerenz, G. Zimmermann, Three dimensional modelling of fractured and faulted reservoirs: Framework and implementation, Chemie der Erde - Geochemistry 70 (SUPPL. 3) (2010) 145–153.

[20] Y. Cherubini, M. Cacace, G. Blöcher, M. Scheck-Wenderoth, Impact of single inclined faults on the fluid flow and heat transport: results from 3-D finite element simulations, Environmental Earth Sciences 70 (8) (2013) 3603–3618.

[21] O. Kolditz, S. Bauer, L. Bilke, N. Böttcher, J. O. Delfs, T. Fischer, U. J. Görke, T. Kalbacher, G. Kosakowski, C. I. McDermott, C. H. Park, F. Radu, K. Rink, H. Shao, H. B. Shao, F. Sun, Y. Y. Sun, a. K. Singh, J. Taron, M. Walther, W. Wang, N. Watanabe, Y. Wu, M. Xie, W. Xu, B. Zehner, OpenGeoSys: an open-source initiative for numerical simulation of thermo-hydro-mechanical/chemical (THM/C) processes in porous media, Environmental Earth Sciences 67 (2) (2012) 589–599.

[22] H. J. Diersch, FEFLOW Finite Element Subsurface Flow & Transoirt Simulation System, Reference Manual, Tech. rep., WASY GmbH Institute for Water Resources Planning and System Research, Berlin (2009).